A quantitative liposome microarray to systematically characterize protein-lipid interactions

Antoine-Emmanuel Saliba[1,6], Ivana Vonkova[1,6], Stefano Ceschia[1], Greg M Findlay[2], Kenji Maeda[1], Christian Tischer[3], Samy Deghou[1], Vera van Noort[1], Peer Bork[1], Tony Pawson[2,5], Jan Ellenberg[4] & Anne-Claude Gavin[1]

Lipids have a role in virtually all biological processes, acting as structural elements, scaffolds and signaling molecules, but they are still largely under-represented in known biological networks. Here we describe a liposome microarray–based assay (LiMA), a method that measures protein recruitment to membranes in a quantitative, automated, multiplexed and high-throughput manner.

The study of lipid interactions with peripheral membrane proteins is of fundamental importance[1–3]. Assays based on the use of artificial, surrogate membranes (liposomes) are popular as they allow lipids to be studied in the context of a membrane bilayer, i.e., under conditions that approximate the *in vivo* situation[4–8]. The lipids are analyzed at close-to-physiological concentrations and in complex, but defined, mixtures with other lipids. These assays are generally quantitative (using, for example, an isothermal titration calorimetry or surface plasmon resonance readout[4,5]) and are thus suited for the study of cooperative mechanisms[6]. However, the fabrication, storage and handling of liposomes are difficult[9]. Protocols designed to produce liposomes[9] cannot be readily scaled up and often require lipid-specific adjustments and the use of nonphysiological buffers[10]. Once in a biological buffer, liposomes are unstable and tend to aggregate and fuse, and the lipids undergo oxidation. Storing liposomes for more than a few days remains problematic[10]. Finally, many of the current liposome-based assays require large amounts of lipids and/or purified proteins, which currently precludes their use in large and systematic analyses.

Here we describe a miniaturized LiMA that uses a fluorescence microscopy readout and is capable of measuring protein recruitment to membranes in a multiplexed and high-throughput manner (**Fig. 1**). Liposomes rapidly self-organize (within 2 min) from lipid mixtures that are soaked up into a thin layer (~50–400 nm) of dried low–melting point agarose upon its hydration in a variety of physiological buffers[11] (**Fig. 1a**,**b**, **Supplementary Fig. 1** and **Supplementary Video 1**). These liposomes are giant (>5 µm) and so are amenable to quantitative analysis by microscopy (**Fig. 1c**,**d**), and their diameters can be further adjusted by varying the thickness of the thin agarose layer (TAL) (**Supplementary Fig. 1b**). The liposomes are restricted to TAL areas where lipids have been applied, and lateral diffusion was not observed (**Supplementary Fig. 1c**). Once assembled, the liposomes remain stably attached to the TAL, and their size and shape do not vary for at least 6 h (data not shown). The procedure is generic and can be used to produce liposomes with a variety of lipids. In total we tested 110 different mixtures, covering the main lipid classes, and all supported the formation of liposomes (**Fig. 2a** and **Supplementary Fig. 2**). We also used fluorescently labeled lipids and genetically encoded fluorescent bioreporters, i.e., lipid-binding domains (LBDs) of known specificity, to confirm the insertion of the main signaling lipids—glycerophospholipids, phosphatidylinositol phosphates, sphingolipids and sterols—in the TAL liposomes (**Fig. 1d** and **Supplementary Fig. 3**).

Next we integrated the TAL into a miniaturized, fluorescence microscopy–based assay capable of measuring protein recruitment to membranes in a multiplexed manner. We sprayed lipid mixtures (400 nl or, in total, 150 nmol of lipids) on the TAL using a Camag thin-layer chromatography spotter (**Supplementary Fig. 4a** and Online Methods), with no cross-contamination (**Supplementary Fig. 1c**), so that they formed 800 × 800–µm^2 spots spaced 200 µm apart (100 spots per cm^2). The signaling lipids were mixed with a carrier lipid, palmitoyl-oleyl-phosphatidylcholine (POPC, an abundant constituent of cellular membranes) and a fluorescently labeled lipid, phosphatidylethanolamine (PE)–Atto 647. Defined amounts of PE bonded to poly(ethylene glycol) (PEGylated PE) were also added to assist liposome formation. The dried, lipid-spotted TAL could be stored under inert gas (argon) for at least 2 months (data not shown). The storage has the advantage of uncoupling the production of the lipid-spotted TAL from the protein-lipid interaction assay. Using soft lithography and fast prototyping fabrication methods[12], we then coupled the lipid-spotted TAL to a circuit of microfluidic channels produced in poly(dimethylsiloxane) (PDMS). This procedure resulted in tight bonding through the TAL that prevented cross-contamination between the channels (**Supplementary Fig. 4b**,**c**). The final device consists of four independent chambers containing 30 different

[1]Structural and Computational Biology Unit, European Molecular Biology Laboratory, Heidelberg, Germany. [2]Samuel Lunenfeld Research Institute, Mount Sinai Hospital, Toronto, Ontario, Canada. [3]Advanced Light Microscopy Facility, European Molecular Biology Laboratory, Heidelberg, Germany. [4]Cell Biology and Biophysics Unit, European Molecular Biology Laboratory, Heidelberg, Germany. [5]Deceased. [6]These authors contributed equally to this work. Correspondence should be addressed to A.-C.G. (gavin@embl.de).

RECEIVED 19 JUNE; ACCEPTED 10 OCTOBER; PUBLISHED ONLINE 24 NOVEMBER 2013; DOI:10.1038/NMETH.2734

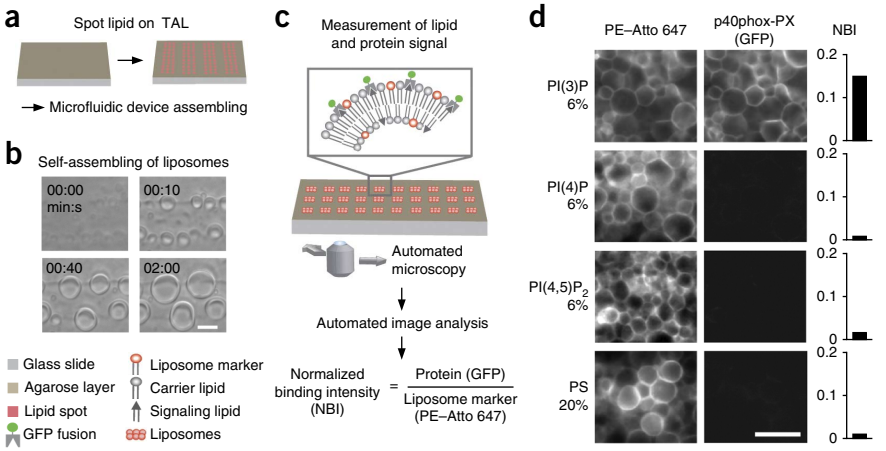

Figure 1 | Liposome microarray–based assay (LiMA) experimental principle and overview. (**a**) Schematic depicting the production and assembly of lipid-spotted thin agarose layers (TALs). (**b**) Time-lapse microscopy showing the self-assembly of liposomes upon hydration of the lipid-spotted TAL. (**c**) Protein-lipid interaction assay. NBI defines the amount of GFP-tagged proteins bound per unit of membrane surface area and normalized by the exposure time. (**d**) Recruitment of the PX domain of p40phox to phosphatidylinositol 3-monophosphate (PI(3)P)-containing membranes. Liposome membranes (PE–Atto 647), bound p40phox-PX (GFP) and NBI (histogram) are represented. PS, phosphatidylserine. Scale bar, 15 µm.

types of liposomes that are made up of different amounts of one or more different signaling lipids (**Supplementary Tables 1** and **2**). About 20 devices can be produced within 1 d. A single device allows the multiplexed analyses of four different signaling proteins with 30 different membranes within ~3 h (**Supplementary Fig. 4c**).

To evaluate the performance of LiMA, we measured the lipid binding profile of a series of peripherally associated membrane proteins that cover six of the most prominent LBDs in eukaryotes: the PH, PX, C1, C2, C2-like and PROPPIN domains (**Fig. 2** and **Supplementary Table 3**). The proteins were produced in *Escherichia coli* or human embryonic kidney 293 (HEK293) cells as GFP-tagged fusions. For each experiment, ~12 µl of cell lysate (from 0.75 to 46.7 pmol of protein) was loaded into individual chambers (**Supplementary Table 3**).

Liposomes were produced upon hydration of the lipid-carrying TALs with buffer. The binding assay started with the introduction of the different GFP-tagged lipid-binding proteins into distinct chambers. Proteins and liposomes were allowed to interact during a 20-min incubation period; incubation was followed by washing, to remove unbound material, and imaging on an automated fluorescence microscopy platform[13]. The GFP-tagged proteins were expressed at substantially different levels, and their membrane affinities varied over a broad range (with the dissociation constant, K_d, ranging from nanomolar to micromolar; **Supplementary Table 3**). To capture this

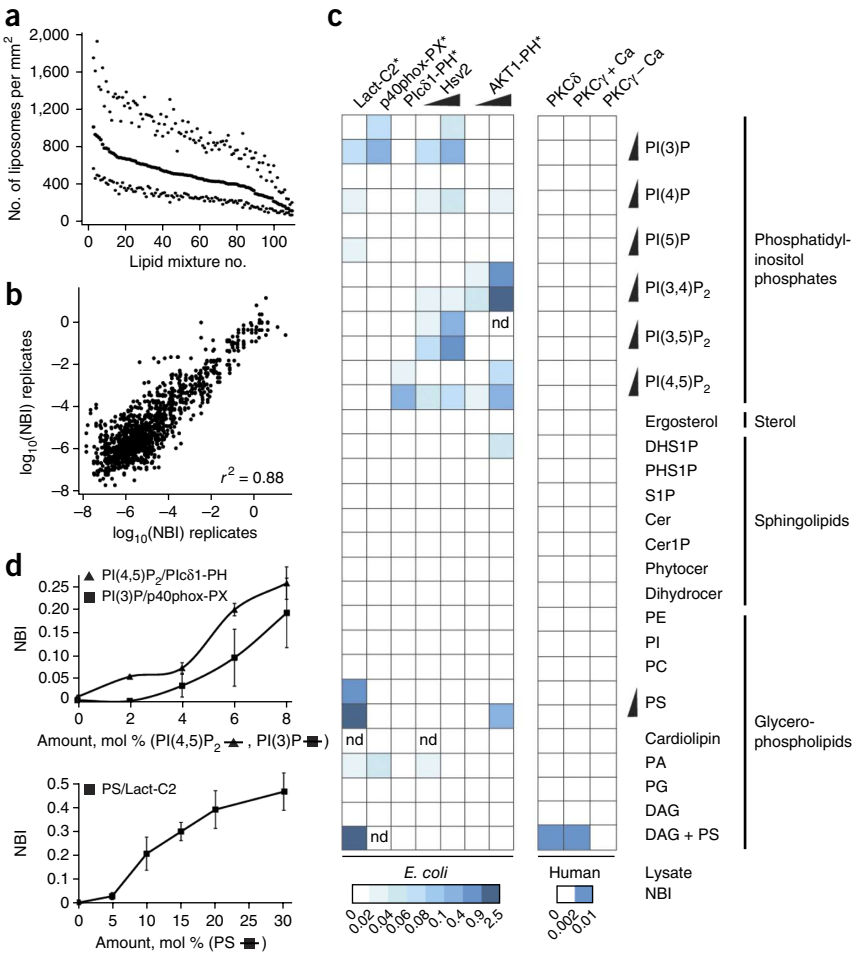

Figure 2 | LiMA quality and validation. (**a**) Efficiencies of liposome formation for 110 representative lipid mixtures. For each lipid mixture the median of >80 replicates is represented (middle curve). The higher and lower data points represent the quartiles at 75% and 25%, respectively. Overall, the lipid mixtures tested produced 479 ± 188 (median ± s.d.) liposomes per mm^2. (**b**,**c**) Binding profiles of seven lipid-binding proteins to 30 types of liposomes (covering 23 different lipid combinations and 7 different concentrations) (n = 3), with reproducibility (**b**) and binding specificity (**c**) shown. The wedges indicate high and low concentrations, respectively. An asterisk (*) indicates that a truncated version of the protein containing only the lipid-binding domain (LBD) was tested. (**d**) Recruitment of LBDs to liposomes containing increasing amounts of the relevant signaling lipid. Values are mean ± s.d. (n = 3). Abbreviations are as in **Figure 1**. Lact, lactadherin; DHS1P, dihydrosphingosine 1-phosphate; PHS1P, phytosphingosine 1-phosphate; S1P, sphingosine-1-phosphate; Cer, ceramide; PE, phosphatidylethanolamine; PI, phosphatidylinositol; PC, phosphatidylcholine; PA, phosphatidic acid, PG, phosphatidylglycerol; DAG, diacylglycerol; nd, not determined. Ca indicates calcium.

substantial physical diversity, we collected the GFP signals at different exposure times and subsequently removed the overexposed pixels (**Supplementary Fig. 5** and Online Methods). The Atto 647 signal (PE–Atto 647) was used to position the liposomes through image segmentation[14]. Only those GFP signals exactly matching the position of the liposomal membranes were analyzed further. Any background signals resulting from, for example, the nonspecific adsorption of proteins to the TAL or from protein aggregation were therefore efficiently filtered out. The Atto 647 intensities reflect the actual surface area of membranes available for binding (i.e., liposome diameters and numbers). The GFP intensities indicate the number of GFP fusions bound to the liposomal membranes. We calculated a normalized binding intensity (NBI)—that is, the ratio of GFP to Atto 647 fluorescence (normalized by the different exposure time)—to reflect the number of GFP-tagged proteins bound per unit of membrane surface area (**Fig. 1** and **Supplementary Fig. 5**). The NBIs are proportional to the amount of interacting proteins recruited to the liposomal membranes (see below) and, if normalized for protein abundance, can be used to quantitatively compare the binding of different proteins.

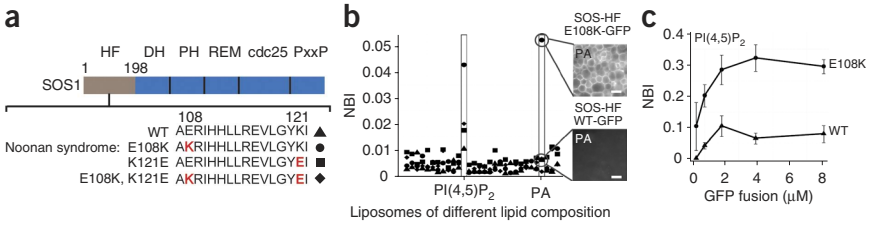

Figure 3 | An E108K mutation in the SOS1 histone-fold domain (SOS-HF) affects its affinity for lipids. (**a**) Schematic of SOS1 and a disease-associated mutation, E108K. (**b**) SOS-HF binding to liposomes of different composition. The symbols are defined in **a**. $PI(4,5)P_2$, phosphatidylinositol 4,5-biphosphate; PA, phosphatidic acid. (**c**) Dose-response curves for the recruitment of SOS-HF wild type (WT) and E108K to $PI(4,5)P_2$-containing liposomes. Values are mean ± s.d. (n = 3). Scale bars, 20 μm.

The procedure is highly reproducible, as the NBIs measured with the same type of liposome in independent experiments correlated well (r^2 = 0.88; **Fig. 2b**). The different LBD-containing proteins showed variations in their NBI depending on their specificity for particular lipids (**Fig. 2c**). Indeed, the NBI profiles confirmed many known specificities[15], such as the interactions between the PX domain of p40phox and phosphatidylinositol 3-monophosphate (PI(3)P); the Hsv2 protein (PROPPIN domain) and both PI(3)P and $PI(3,5)P_2$; the C2-like domain of lactadherin and phosphatidylserine (PS); the PH domain of AKT1 and the product of the phosphatidylinositol-3-kinase ($PI(3,4)P_2$) or PS; and the PH domain of phospholipase Cδ1 and $PI(4,5)P_2$. The assay is sensitive, as we could measure interactions with less than 1 pmol of protein (**Supplementary Table 3**), and quantitative, as the NBIs for an interacting protein-lipid pair were proportional to the amount of lipid and protein present in the assay (**Fig. 2d** and **Supplementary Fig. 6**). It also captures cooperative binding mechanisms such as the membrane recruitment of protein kinase C-δ (PKCδ, two C1 domains and one C2 domain) that requires both diacylglycerol (DAG) and PS[16] and the calcium-dependent recruitment of protein kinase C-γ (PKCγ) to DAG-and-PS–containing membranes[16].

We next assessed whether LiMA can be used to measure discrete changes in binding affinities. Son-of-sevenless (SOS1) is a guanine nucleotide exchange factor with multiple lipid- and protein-binding domains that integrate complex regulatory inputs and thus control activation of the Ras GTPase[17] (**Fig. 3a**). An E108K mutation in the amino-terminal histone-fold domain of SOS1 (SOS-HF) increases its affinity for phosphatidic acid (PA)[18] and causes Noonan syndrome, a developmental disorder that includes heart malformation. The effect of E108K mutation on SOS-HF binding affinities is abolished by the introduction of a K121E mutation. In our assay, wild-type SOS-HF bound weakly and specifically to both PA and $PI(4,5)P_2$ (ref. 18; **Fig. 3b**,**c** and **Supplementary Fig. 6**). The apparent affinity of SOS-HF containing the disease-associated E108K mutation was substantially increased for both PA and $PI(4,5)P_2$ (the respective NBIs were two- and fivefold higher), which is consistent with the hypotheses that the two lipids occupy the same, or overlapping, binding sites and that increased binding of SOS1 to membrane lipids leads to Noonan syndrome.

LiMA can potentially be extended further to deliver an interaction profile that is scalable to the proteome or lipidome levels. Its development is timely with the functional genomics resources now available, such as genome-wide collections of cell lines expressing GFP fusions[19,20]. LiMA allows the systematic mixing of lipids and probing for cooperative mechanisms. In addition, the assay should be readily adaptable to other readouts. If LiMA is used in combination with mass spectrometry, unlabeled proteins could be measured. Integration with advanced optical methods, such as total-internal-reflection fluorescence microscopy or two-photon excitation microscopy, may also make it possible to acquire equilibrium dissociation constants (K_d). Finally, further development of LiMA should allow studies on the disruption of protein-lipid interactions by small molecules.

METHODS

Methods and any associated references are available in the online version of the paper.

Note: Any Supplementary Information and Source Data files are available in the online version of the paper.

ACKNOWLEDGMENTS

We dedicate this paper to T.P. We are grateful to C. Merten, M. Kaksonen, A. Galih, K. Kugler, C. Besir, M. Hsiung, M. Skruzny and the Protein Expression and Purification Core Facility for expert help and the sharing of reagents. We thank M. Mall (European Molecular Biology Laboratory) for the PKCγ and PKCδ (in the pEGFP-N3 vector). We also thank J.E.'s and other members of A.-C.G.'s groups for continuous discussions and support. This work was partially funded by the German Federal Ministry of Education and Research (BMBF; 01GS0865) in the framework of the IG-Cellular System genomics to A.-C.G. K.M. was supported by the Danish Natural Science Research Council (09-064986/FNU). A.-E.S. is supported by the European Molecular Biology Laboratory and the EU Marie Curie Actions Interdisciplinary Postdoctoral Cofunded Programme.

AUTHOR CONTRIBUTIONS

A.-E.S., I.V., J.E., V.v.N., P.B., T.P. and A.-C.G. designed the research, discussed the results and/or advised on the analyses; A.-E.S., I.V., S.C. and S.D. conducted the experiments and performed the analyses; G.M.F., K.M. and C.T. provided key technical expertise with instrumentation, protocols and reagents; and A.-E.S., I.V. and A.-C.G. wrote the manuscript with support from all the authors.

COMPETING FINANCIAL INTERESTS
The authors declare competing financial interests: details are available in the online version of the paper.

1. Di Paolo, G. & De Camilli, P. *Nature* **443**, 651–657 (2006).
2. Gallego, O. *et al. Mol. Syst. Biol.* **6**, 430–444 (2010).
3. Leonard, T.A., Różycki, B., Saidi, L.F., Hummer, G. & Hurley, J.H. *Cell* **144**, 55–66 (2011).
4. Narayan, K. & Lemmon, M.A. *Methods* **39**, 122–133 (2006).
5. Wu, H.J. *et al. Nat. Methods* **9**, 1189–1191 (2012).
6. Jung, H., Robison, A.D. & Cremer, P.S. *J. Struct. Biol.* **168**, 90–94 (2009).
7. Majd, S. & Mayer, M. *Angew. Chem. Int. Edn Engl.* **44**, 6697–6700 (2005).
8. Estes, D.J., Lopez, S.R., Fuller, A.O. & Mayer, M. *Biophys. J.* **91**, 233–243 (2006).
9. Walde, P., Cosentino, K., Engel, H. & Stano, P. *ChemBioChem* **11**, 848–865 (2010).
10. Jesorka, A. & Orwar, O. *Annu. Rev. Anal. Chem. (Palo Alto Calif.)* **1**, 801–832 (2008).
11. Horger, K.S., Estes, D.J., Capone, R. & Mayer, M. *J. Am. Chem. Soc.* **131**, 1810–1819 (2009).
12. Duffy, D.C., McDonald, J.C., Schueller, O.J. & Whitesides, G.M. *Anal. Chem.* **70**, 4974–4984 (1998).
13. Neumann, B. *et al. Nat. Methods* **3**, 385–390 (2006).
14. Carpenter, A.E. *et al. Genome Biol.* **7**, R100 (2006).
15. Lemmon, M.A. *Nat. Rev. Mol. Cell Biol.* **9**, 99–111 (2008).
16. Rosse, C. *et al. Nat. Rev. Mol. Cell Biol.* **11**, 103–112 (2010).
17. Findlay, G.M. *et al. Cell* **152**, 1008–1020 (2013).
18. Yadav, K.K. & Bar-Sagi, D. *Proc. Natl. Acad. Sci. USA* **107**, 3436–3440 (2010).
19. Huh, W.K. *et al. Nature* **425**, 686–691 (2003).
20. Hutchins, J.R. *et al. Science* **328**, 593–599 (2010).

ONLINE METHODS

Recombinant protein expression. Synthetic genes encoding protein domains were codon optimized for expression in *E. coli* (Entelechon) (Plcδ1-PH, AKT1-PH, p40phox-PX). The gene encoding full-length Hsv2 was cloned from the *Saccharomyces cerevisiae* genome (forward primer, aaaaggatccatggatgttcgtcga cctataagg; reverse primer, aaaagctagcaagctctctccatgattctctcac). The gene encoding the C2 domain of lactadherin was PCR amplified from the p416-GFP-Lact-C2 vector (Haematologic Technologies) (forward primer, ttttggatcctgcactgaacccctaggcctgaagg; reverse primer, ttttaagcttacagcccagcagctccacg; for sequence details see **Supplementary Table 3**).

All genes except those encoding PKCγ and PKCδ were then inserted into the pETM11 vector, and proteins were expressed as N-terminal His6-SUMO3 and C-terminal superfolder GFP (sfGFP)[21] fusions in *E. coli* (BL21 STAR, Invitrogen). Cells were grown in autoinducing ZY medium at 37 °C up to $OD_{600} \approx 2$. Subsequently, the temperature was shifted to 15 °C, and protein was produced overnight for 14–15 h. Cells were pelleted at 3,000*g* for 20 min and washed in cold PBS. Final pellets (volume ≈ 100 µL) were snap frozen in liquid nitrogen and stored at −80 °C.

The genes encoding PKCγ and PKCδ, cloned into a pEGFP-N3 vector (kind gift from M. Mall, EMBL), were transiently expressed as C-terminal EGFP fusions in HEK293 cells (ATCC-CRL-1573) after transfection with 6 µg DNA per 15-cm plate using Lipofectamine 2000 (Invitrogen). Cells were grown in DMEM (Dulbecco's modified Eagle's medium) complemented with 10% serum (FBS, Invitrogen) at 37 °C up to 80% confluence.

Preparation of cell extract from *E. coli* cells. Cell lysis was performed in lysis buffer (10 mM HEPES, 150 mM NaCl, 0.5 mM DTT, protease inhibitors cocktail (Roche) and nuclease (Novagen), pH 7.4) by mild sonication (100 µL pellet lysed in 500 µL lysis buffer). The final cell extract was obtained by centrifugation for 20 min at 16,000*g*. Expression level and protein solubility were evaluated on both a Coomassie stained gel and a western blot with anti-GFP antibody (MACS Miltenyi Biotec, cat no. 130-091-833, dilution 1:10,000). Fluorescence intensity of GFP tagged protein in the cell extract was measured on a microplate reader (BioTek) at excitation and emission wavelengths of 485 nm and 528 nm, respectively.

Preparation of cell extract from HEK293 cells. Cells were washed in PBS and lysed in ice-cold 500 µL hypotonic buffer (10 mM Tris, pH 7.4, 10 mM NaF, protease inhibitors cocktail) 20 min on ice. Cells were passed through a 30-gauge needle 15 times, and a clear lysate was obtained after centrifugation (16,000*g*, 10 min). NaCl concentration was adjusted to 150 mM, and the lysate was stored at −80 °C. In the case of PKCγ, $CaCl_2$ was added to final concentration of 2 mM or EDTA to 10 mM.

Protein purification. Cell pellets were resuspended in lysis buffer (50 mM Tris, pH 7.5, 500 mM NaCl, 20 mM imidazole, 0.5 mM DTT, protease inhibitors cocktail and nuclease). Cells were lysed by sonication, and the soluble fraction was obtained by centrifugation (39,000*g* for 45 min). The N-terminal His6-SUMO3–tagged protein was captured on the Ni-NTA agarose (Qiagen). After a wash with the lysis buffer, the protein was eluted in 50 mM Tris, pH 7.5, 250 mM NaCl and 300 mM imidazole and dialyzed against 10 mM HEPES, pH 7.4 and 250 mM NaCl overnight. The His6-SUMO3 tag was cleaved with the SenP2 protease during the dialysis, and the undigested protein and cleaved tag were removed using the Ni-NTA agarose. The protein was further purified on the Superdex 200 gel filtration column (GE Healthcare) pre-equilibrated with 10 mM HEPES, pH 7.4 and 250 mM NaCl. For use in the assay, the NaCl concentration of the purified proteins was adjusted to 150 mM by dilution.

Estimation of GFP fusions concentration in cell extract. Purified Plcδ1-PH-sfGFP was diluted to seven different concentrations ranging from 0.5 µM to 15 µM (0.5, 1, 2, 4, 8, 10 and 15). The fluorescence intensity of each of these dilutions was then measured on microplate reader (BioTek) at excitation and emission wavelengths of 485 nm and 528 nm, respectively. Values obtained from microplate reader for all different Plcδ1-PH-sfGFP concentrations allowed us to plot a standard curve, which was used to calculate the concentrations of GFP fusions in cell extract.

Lipid spotting on TAL. Coverslips (30 × 45 mm^2, #1; Menzel) were washed briefly with acetone and isopropanol, overnight in 1% (v/v) Hellmanex III (Hellma), and thoroughly in dH_2O under sonication for 10 min; they were then dried under a stream of argon.

The TAL (thin agarose layer) was formed by dip-coating the glass slides in a 1% (w/v) agarose solution (low–melting temperature agarose, Type IX-A) and dried overnight at room temperature (RT). Coverslips with TAL were stored at RT. Agarose layer height was measured by profilometry (Dektak 8, Veeco Instruments). Homogeneity of TAL on a coverslip was checked through independent measurements (**Supplementary Fig. 1**).

Initially, spotting of lipid mixtures on a bare TAL led to cross-contamination between the spotted lipid mixtures. This was overcome by spotting lipids on a TAL covered with an engineered membrane made of the thiol-ene–based resin NOA81 (Norland Optical) (**Supplementary Fig. 4**) that introduces boundaries between neighboring spots and localizes the spots following a predefined pattern (**Supplementary Fig. 1**). A mask bearing a pattern of 800-μm^2 squares with 1,000-µm center-to-center distance was designed using QCAD software and printed at a resolution of 24,000 d.p.i. (Selba) on a poly(ethylene terephthalate) film. The mask features were transferred into a negative resist SU8-2,075 (Microchem) spin coated on a silicon substrate, forming a master with holes of 800 μm^2 and a height of 65 µm. A replica of the master was fabricated by pouring a solution of poly(dimethylsiloxane) (PDMS) (Sylgard 184, Dow Corning) mixed at 10:1 base:curing agent and cured 3 h at 65 °C before being peeled. The replica was impermanently bonded to a bare glass slide, and the solution of liquid NOA81 prepolymer was injected between the empty space and the glass slide and solidified after UV illumination[22]. After UV illumination, the PDMS replica could be released, and the NOA81 membranes could be detached from the glass slide using a scalpel. The membranes were placed on the agarose-coated coverslip, where they adhered via electrostatic bonding. The membranes were removed from the coverslip after spotting and could be reused after sonication in isopropanol.

All lipid mixtures were prepared in chloroform-based solvent (see **Supplementary Table 1**) and stored in 1.5 mL glass vials (Sigma). The different lipid mixtures each corresponded to a different lipid vial with solvent and corresponding lipids. All lipid mixtures

were completed with PE–Atto 647 (0.1% mol ratio) to ensure autofocusing during automated microscopy and PE-PEG350 (0.5% mol ratio) that, in addition to agarose, further helped the generation of liposomes. In the case of PI(3,4,5)P_3 liposomes (**Supplementary Fig. 3**), PE-PEG2,000 (5% mol ratio) was used. All lipid solutions were stored under argon at –20 °C. Under these storage conditions, solutions could be kept for more than 2 months without noticeable degradation (which was checked by lipid MS/MS).

Lipids mixtures were spotted using a syringe-driven spotter (Automatic TLC-spotter4, Camag) on TALs covered with the protective membrane under an inert atmosphere. 20 coverslips were spotted in parallel. After lipid spotting, coverslips were stored under inert atmosphere before being bound to a PDMS device (**Supplementary Fig. 4b**,**c**).

Microfluidics device fabrication. Devices were fabricated using standard soft-lithography protocol[23]. The master used to pattern the device (four chambers) was prepared using standard photolithography with SU8-2,150 (Microchem) spin coated onto a 4-inch silicon wafer. The devices were modeled, using the master as a mold, with a 10:1 mixture of PDMS:curing agent (Sylgard 184 silicone elastomer) and cured 3 h at 65 °C.

To bond the spotted TAL with the PDMS devices (**Supplementary Fig. 4b**), we used a PDMS prepolymer (i.e., not reticulated PDMS; 2:1 mixture of silicone elastomer:curing agent diluted 3× (vol:vol) in hexane) as an 'adhesive'[24]. The adhesive was spin coated on a coverslip (2,200 r.p.m., 30 s) previously washed with acetone. The PDMS devices were inked with the adhesive by dipping and peeling off after a few seconds. The PDMS devices were then placed in contact with the lipid-spotted agarose-coated coverslip and immediately placed under inert atmosphere (argon atmosphere). The microfluidics devices (i.e., the spotted TALs bonded to the PDMS devices) were stored at 4 °C in a Mylar bag (Sorbent Systems).

Experimental procedure. Liposomes were formed by injecting the assay buffer (10 mM HEPES, 150 mM NaCl) in the chambers using a Hamilton syringe and incubating for 20 min. The samples were subsequently injected in the chambers using a syringe pump (KD scientific). After 20 min, the chambers were washed for unbound proteins using the assay buffer. The microfluidics device was then coupled to the microscope for imaging. The analysis was not affected by vertical movement of the liposomes. Indeed, after ~5 min the liposomes and TAL were fully swollen and remained stable for at least 6 h. We did not observe liposome rupture during the time of the assay.

Image acquisition and image processing. For all experiments two sets of images were acquired: one set for Atto 647, representing the position of liposomes, and second set for GFP, representing protein-lipid binding events (**Supplementary Fig. 5**). Images were acquired with an automated epifluorescence microscope (IX-81; Olympus) (objective 20×/0.7 NA) and a CCD camera (Hamamatsu Orca-R2). We used a xenon lamp (MT-20, Olympus) with the following filters. (i) For GFP we used a beam-splitter long-pass with edge at 495 nm; excitation, band-pass between 450 nm and 490 nm; and emission, band-pass between 500 nm and 550 nm. (ii) For Atto 647 we used a beam-splitter long-pass with edge at 660 nm; excitation, band-pass between 540 nm and 650 nm; and emission, band-pass between 667 nm and 735 nm.

Atto 647 images were taken at one constant exposure time: 3 ms. So that we captured a broad range of binding affinities of tested proteins, nine different GFP exposure times were taken for each experiment, ranging from 5 ms (for strong binders and/or high-concentration proteins) to 1,000 ms (weak binders and/or low-concentration proteins). Exposure times of 5 ms, 10 ms, 30 ms, 50 ms, 75 ms and 100 ms were used for the GFP fusions expressed in *E. coli*. For the GFP fusions expressed in HEK293 extracts (lower expression levels), three additional exposure times were added (200 ms, 300 ms and 1,000 ms).

Image processing was done with an open-source image analysis software[14] (http://www.cellprofiler.org/). The first step in the image processing pipeline consisted of filtering out the background using the top-hat morphological filter. The resulting filtered Atto 647 images were subsequently used for image segmentation to retrieve the position of liposome membranes. We used this information to define the surface area (we call this the "mask" in **Supplementary Fig. 5**) that contains pixels carrying information on liposome–GFP-fusion interactions. Only pixels matching the mask were further analyzed. Filtered Atto 647 images were also used to determine the centers of the liposomes. This information was used to estimate the number of liposomes (**Fig. 2a**).

Subsequently, overexposed pixels were identified in all images. Each GFP image within a series (i.e., different exposure times for the same GFP-fusion–liposome pair) was paired with its respective Atto 647 image (3 ms). The corresponding overexposed pixels within the pairs (Atto 647 (3 ms) and GFP (*x* ms)) were removed from both images (i.e., set to 0). This process—i.e., pairing images and removing corresponding overexposed pixels from both of them (Atto 647 and GFP)—resulted in exactly the same number of nonoverexposed pixels in both paired images. For each pair of images, we thus extracted the following information: (i) the number of nonoverexposed pixels overlapping with the mask and (ii) the corresponding mean GFP and Atto 647 intensities.

For the images in **Figures 1d** and **3b**, we applied the settings described in the **Supplementary Note** using ImageJ.

Calculation of mean NBI values. For each exposure time, we calculated the ratio between the mean GFP and Atto 647 intensities (**Supplementary Fig. 5a**). Exposure times leading to images with high numbers of overexposed pixels (i.e., for which the reduction of analyzed pixels was >5% of that for the previous exposure times) were not further considered (**Supplementary Fig. 5c**, "strong binder"). For each remaining exposure time, we defined a normalized binding intensity (NBI) as the GFP–versus–Atto 647 intensities normalized for (divided by) the exposure time. The NBIs were roughly constant across all exposure times (**Supplementary Fig. 5c**), and here we used their mean as a final measure of binding intensity. The final NBIs from different proteins can thus be compared quantitatively with each other, given, of course, that NBIs are further normalized for protein abundance (i.e., different expression levels).

21. Pédelacq, J.D., Cabantous, S., Tran, T., Terwilliger, T.C. & Waldo, G.S. *Nat. Biotechnol.* **24**, 79–88 (2006).
22. Bartolo, D., Degré, G., Nghe, P. & Studer, V. *Lab Chip* **8**, 274–279 (2008).
23. Qin, D., Xia, Y. & Whitesides, G.M. *Nat. Protoc.* **5**, 491–502 (2010).
24. Wu, H., Huang, B. & Zare, R.N. *Lab Chip* **5**, 1393–1398 (2005).

doi:10.1038/nmeth.2734